In situ growth of hexagonal prism-like $Ni(OH)_2$ microrods on nickel foam as binder-free electrodes

Gang Li[1], Zhuoqing Chang[1], Tingyu Li[1*] and Kaiying Wang[1, 2*]

[1] *MicroNano System Research Center, College of Information and Computer & Key Lab of Advanced Transducers and Intelligent Control System (Ministry of Education), Taiyuan University of Technology, Taiyuan, 030024, China*
[2] *Department of Microsystems-IMS, University of South-Eastern Norway, Horten, 3184, Norway*

* Email: litingyu@tyut.edu.cn, Kaiying.Wang@usn.no

Abstract: In this paper, we report *in situ* growth of hexagonal prism-like $Ni(OH)_2$ microrods via one-step hydrothermal process, which nickel foam is directly oxidized in a high concentration hydrogen peroxide (H_2O_2) solution without additional nickel sources, surfactant, or post-treatment. The nickel foam not only serves as a nickel source but also as 3D scaffold for $Ni(OH)_2$ growth to form binder-free electrodes. The *in situ* growth can ensure close contact between conductive Ni foam substrate and as-formed $Ni(OH)_2$ microrods, providing efficient electron collection paths and electrochemical stability. Mass loading of $Ni(OH)_2$ on nickel foam could be tailored by adjusting the concentration H_2O_2. Possible growth mechanism of hexagonal prism-like $Ni(OH)_2$ microrods are discussed to understand the morphologies under various H_2O_2 concentrations. When works as a binder-free electrode, the $Ni(OH)_2$-coated nickel foam exhibits an remarkable areal capacitance ~ 1.598 C cm^{-2} (560 C g^{-1}) at a current density of 1 mA cm^{-2}, relatively high rate capability with 57.14% areal capacitance nickel foam retained at 10 mA cm^{-2}, as well as better cycling stability with 72.9% areal capacitance remained after charge-discharge 3000 cycles. Such superior performance demonstrate that $Ni(OH)_2$ microrods *in situ* grown on metallic nickel foam substrate might be a potential electrode material for electrochemical capacitors.

Key words: Hydrothermal synthesis, nickel hydroxide microrods, supercapacitor, Nickel foam

1. Introduction

Supercapacitor is considered as an efficient, energy-saving, environmentally friendly, energy storage device with high power density, long service life, fast and high current charging [1-4]. Supercapacitors are classified into either electric double layer capacitors (EDLCs) or pseudocapacitors, according to their charge storage mechanisms. Generally, EDLCs employ carbon−based materials to electrostatically store charges through reversible ion adsorption/desorption at the interface between electrode surface and electrolyte [5]. Pseudocapacitors utilize transition metal oxides/hydroxides/nitrides [1, 4, 6] or conducting polymers [7] to achieve high energy storage capacity via fast and reversible redox processes occurring on the surface of electrodes, such as RuO_2 [8], MnO_2 [9], NiO [10], and $Ni(OH)_2$ [6, 11-13]. However, they always suffer from poor electrical conductivity and low electrochemical stability, which cause gradual loss of capacitance.

Benefiting from its unique structure and high theoretical specific capacitance, nickel hydroxide ($Ni(OH)_2$) is cost effective and is available in various morphologies, making it a promising battery−type electrode candidate among various pseudoactive materials. However, actual specific capacitances are much lower than their theoretical value due to inefficient usage of active material resulted from limited surface area and poor electrical conductivity [13]. Recently, three-dimensional (3D) $Ni(OH)_2$ materials with high surface area have been explored to achieve high specific capacitances. For instance, hierarchical $Ni(OH)_2$ hollow spheres [14], α-$Ni(OH)_2$ nanosheets [15], $Ni(OH)_2$-carbon composites [16] have been scrutinized. However, these high-surface-area 3D pseudoactive materials have to be coated on a current collector. The additional binder linking the materials onto a current collector will increase the internal resistance and further inevitably degrade overall specific capacitance [17]. As a common conductive substrate (current collector) for active materials, nickel foam has been widely adopted due to light weight, low cost, dimensional stability, high electrical and thermal conductivity. Therefore, several methods, such as hydrothermal treatment [18], electrodeposition [16], and chemical bath deposition [19], have been conducted to directly grow $Ni(OH)_2$ on nickel foams to decrease the internal resistance caused by additional binder. However, the foregoing methods require precise control of nucleation and growth

of the deposits, additional nickel sources and accurate temperature. The electrodes often have a defective structure and do

not ensure efficient charge transfer [13]. On the other hand, additional materials grown on nickel foam may suffer from relatively weak adhesion between active materials and current collector, resulting in a poor electrochemical stability due to the gradual loss of mass.

Herein, we report direct oxidation of the surface of nickel foam to grow hexagonal prism-like $Ni(OH)_2$ microrods by a one-step hydrothermal method. The nickel foam not only serves as nickel source but also as 3D scaffold for $Ni(OH)_2$ growth to from a binder-free electrode. The *in situ* growth can provide close contact between conductive Ni foam substrate and as-formed active materials to enhance the electrical conductivity and electrochemical stability. Then surface morphology of $Ni(OH)_2$-coated nickel foams have been optimized for high-performance supercapacitor electrodes by adjusting hydrogen peroxide concentration.

2. Experimental

All chemicals were of analytical grade and used without further purification. Five pieces of nickel foams (Purity of 99.99%, thickness of 1.0 mm, pore size of 110 PPI) were cut into ~ 2.0 cm × 4.0 cm as hydrothermal raw materials, followed by ultrasonic cleaning in acetone, 1 M HCl, absolute ethanol, and deionized water for 10 min. The nickel foams were vacuum-dried at 60 ℃for 12 h. The mass of the nickel foams before hydrothermal process were weighed to be 2.478, 2.560, 2.532, 2.653, 2.510 g, respectively. The cleaned nickel foams were suspended by nickel wires and immersed in 50 mL of 5 wt%, 10 wt%, 15 wt%, 20 wt%, and 25 wt% H_2O_2 aqueous solution for ten minutes, respectively. Then they were transferred into 100 mL Teflon−lined stainless autoclave, and kept at 180 ℃for 24 h. After cooling down to room temperature, the nickel foams were removed and cleaned with ethanol and distilled water, and vacuum-dried at 60 ℃for 12 h. Finally, the mass of the five nickel foams was turned to be 2.483, 2.567, 2.540, 2.663, 2.520 g, respectively. Thus, the mass loading of active materials on nickel foams were calculated to be 1.89, 2.30, 2.90, 3.20 and 3.48 mg cm^{-2}, respectively. They were labeled wt1, wt2, wt3, wt4 and wt5, respectively.

Morphology and structure of the nickel foams were characterized by Scanning Electron Microscope with Energy Dispersive X-ray spectroscopy (FESEM/EDX, SU8010). Their crystalline structures were

identified by X-raydiffraction (XRD)analysis using a RigakuD/MAX−3B automated X-ray diffractometer

system with Cu-Kα radiation at 40 kV and 40 mA, and 2θ ranging from 10 to 70 at room temperature. The chemical compositions of as-formed pseudoactive materials were further examined by X-Ray photoelectron spectroscopy (XPS, Thermo ESCALAB 250). Electrochemical properties of the electrodes $Ni(OH)_2$ were tested based on cyclic voltammetry (CV), galvanostatic charge/discharge (GCD) and electrochemical impedance spectroscopy (EIS) using a three-electrode electrochemical workstation (Zahner), where the nickel foams served as a working electrode, platinum plate and Hg/HgO as counter and reference electrodes. The CV curves were respectively recorded from 0 to 0.8 V at scan rates of 1, 2, 5, 10, 20, and 50 mV s^{-1} at room temperatures. The GCD measurements were performed in the potential between 0 and 0.55 V at different current densities of 1, 2, 5, 10, 15, and 20 mA cm^{-2}. The cycling stability was evaluated by GCD measurements at a current density of 10 mA cm^{-2} for 1000 cycles. The EIS measurements were conducted by applying an AC voltage with 5 mV amplitude in frequency range of 0.01 Hz to 100 kHz. The nominal area of $Ni(OH)_2$ electrodes immersed in the electrolyte was ~ 2.0 cm^{-2}.

3. Results and discussion

Fig.1 shows fabrication procedure and photos of pristine/processed nickel foams by 0, 5, 10, 15, 20, 25 wt% H_2O_2, respectively. It can be seen that the nickel foams color are changed from metallic grey to dark green as increasing the H_2O_2 concentration. The green color is characteristic behavior of crystalline nickel hydroxide β-$Ni(OH)_2$ [17]. During hydrothermal process, hydrogen peroxide solution acts as the strong oxidant, very unstable when heated over 153 °C and violently disintegrates into water and oxygen [20]. The possible formation mechanism of hexagonal prism-like $Ni(OH)_2$ rods could be described as the following two processes: (1) The Ni atoms on the surface of nickel foam aree firstly oxidized into hexagonal prism-like $Ni(OH)_2$ plates by as-formed oxygen. (2) With increasing reaction time, the as-formed hexagonal prism-like $Ni(OH)_2$ plates were further grown into hexagonal prism-like rods at high vapor pressure and reactant concentrations.

Fig. 2 a-e present SEM images of the Ni foams after hydrothermal process with H_2O_2 concentration equal to 5 wt%, 10 wt%, 15wt%, 20wt%, and 25wt% respectively. The surface of pristine 3D macro-porous nickel foams is smooth and free of nickel oxides. Obviously, the surface of the nickel foam has

been modified to some extent after the processes, while still maintaining 3D macrospores structure of the pristine

nickel foam. Fig. 2a shows a flat surface morphology without any microrods on the nickel foam surface with H_2O2 concentration ~5 wt%, indicating low concentration H_2O_2 could not provide enough oxidation ability to form microrods. Fig. 2b presents several microrods grown on the nickel foam as the concentration is about 10 wt%, indicating medium concentration H_2O_2 could form microrods but with quite slow growth rate. Fig. 2c shows that large amount of microrods were formed on nickel foam, indicating the growth rate was obviously accelerated as the concentration is 15 wt%. Fig. 2d shows that there are quite compact and uniform microrods on nickel foam with proper growth rate as the concentration is 20 wt%. The SEM image of sample wt4 at high magnification (Fig. 2e) reveals that the $Ni(OH)_2$ rods with hexagonal prism-like micro structure. Fig. 2f shows highly dense microrods agglomerated together on nickel foam, indicating the extremely high growth rate as the concentration is 25 wt%. It is concluded that the morphology of nickel foam after processing is strongly dependent on the concentration of H_2O_2 aqueous solution, and high concentration of H_2O_2 intensifies the oxidation of nickel foam. Thus, the mass loading of active materials on nickel foam could be tailored by adjusting the concentration of H_2O_2. Furthermore, the spaces between the formed microrods play a critical role in the charge transport of electrons and ions. The large space could facilitate the charge transport, with low mass loading of active materials. While small space could increase the mass loading of active materials, with low charge transport ability.

Fig. 3 shows an X-ray diffraction (XRD) pattern of the sample wt4. The diffraction peaks at 19.6°, 33.4°, 38.8°, 52.2°, 59.2°, and 62.7° are indexed to (001), (100), (101), (012), (110), (111) planes of the β-$Ni(OH)_2$ (JCPDS no.14−0117) [21]. While the weak diffraction peaks at 29.9°, 31.5° and 35.0° are indexed to (−222), (013), (400) planes of the $Ni(PO_3)_2$ (JCPDS no.28−0708) [22]. The co−existence of element P may come from the phosphoric acid, because the hydrogen peroxide solution always contains a small amount of phosphate, which is used as an acidifier in the preparation of hydrogen peroxide as well as a stabilizer of hydrogen peroxide [23]. Therefore, a small amount of $Ni(PO_3)_2$ was possibly produced during the hydrothermal process.

X-ray photoelectron spectroscopy (XPS) was carried out to investigate the detailed elemental composition and the oxidation state of the as-synthesized $Ni(OH)_2$ microrods. The XPS survey spectrum (Fig. 4a) reveals the presence of Ni *2p*, O *1s*, P *2p* and C *1s*, among which C is contamination that

accumulated during the storage of the sample in air. The high-resolution Ni *2p* spectrum (Fig. 4b) presents two main peaks at 857.5 eV and 875.1 eV associated with Ni *2p*3/2 and Ni *2p*1/2, respectively, together with two satellite peaks at 879.6 eV and 861.4 eV, which is typical characteristic of $Ni(OH)_2$ and $Ni(PO_3)_2$ [11, 22]. The strong peaks at 530 eV and 531.6 eV, in the high−resolution O *1s* spectrum (Fig. 4c), correspond to bound hydroxide groups (OH^-) and P–O–P bridging oxygen atoms [11, 24]. In the high-resolution P *2p* (Fig. 4d), the peaks located at 134.9 eV and 138.9 eV are related to P–O species, revealing the existence of the $Ni(PO_3)_2$ component [25], which is consistent with the XRD results.

Stimulated by 3D architecture of *in situ* grown hexagonal prism-like $Ni(OH)_2$ microrods, it is directly served as binder- and conductive- agent-free electrodes. CV curves of the nickel foams oxidized by various concentrations of H_2O_2 aqueous solution recorded at a scant rate of 20 mV s^{-1} are presented in Fig. 5a. The CV curves consist of a pair of redox peaks, indicating that the measured capacitances differ from those of EDLCs. When increasing the H_2O_2 concentration from 0 to 25 wt%, the sample wt4 (20 wt%) shows the highest oxidation (~ 0.656V)and lowest reduction (~ −0.184 V) peaks on the C−Vcurves. The nickel foam wt4 electrode has the largest closed curve area, thus, 20% hydrogen peroxide aqueous solution might be the optimal concentration for the *in situ* hydrothermal process. The high capacitance might result from the increased accessible surface area between the $Ni(OH)_2$ active material and electrolyte. Furthermore, CV curves of the sample wt4 at scan rates varying from 1 to 50 mV s^{-1} are shown in Fig. 5b. The redox currents of the electrodes increase with the rising scan rate, and the redox peak positions are shifted to large potential separation. In principal, the lower scan rate leads to more utilization of active material. With increasing the scan rate, the limited ion diffusion rate leads to a decrease in the active material utilization. However, the shapes of CV curves remain unchanged, indicating that the material has high faraday reaction reversibility. Plotting log (peak current, *i*) versus log (scan rate, *v*) produces a straight line with a slope of

0.497 (very close to 0.5, Fig. 5c), which indicates that such hexagonal prism-like microrods are battery-type electrode materials [2].

The phenomenon was further illustrated by the GCD tests obtained at a current density of 5 mA cm^{-2}. As shown in Fig. 5d, all curves display a triangular deviation, showing that the capacitance comes from the Faradaic redox reactions. Remarkably, the discharging time of the nickel foam wt4 shows an optimal value

comparable with that of other processed nickel foams, indicating that the sample wt4 achieved the highest specific capacitance among the five electrodes. Fig. 5e presents the results of GCD curves of the nickel foam wt4 at various current densities varying from 1 to 20 mA/cm^{-2} with a potential window ranging from 0 to 0.55 V (vs. Hg/HgO reference electrode). The shape of all the charging and discharging curves is far from ideal straight line due to the impact of faradic reaction process. The areal capacitance (C_a) of the battery-type electrodes can be calculated from the discharge times according to the following formula [26, 27]:

$$C_a = i_a * \Delta t \quad (1)$$

Where i_a (A cm^{-2}) represents the current density during the discharge process, and Δt (s) is discharge time. The calculated areal capacitance as a function of the discharge current density was plotted in Fig. 5f. Similarly, the nickel foam wt4 achieved the highest capacitance among the five electrodes. The areal capacitance is 1.598 C cm^{-2} (584 C g^{-1}) at 1 mA cm^{-2} and 1.120 C cm^{-2} (350 C g^{-1}) at 10 mA cm^{-2}. The areal capacitance in terms of 2.91 F cm^{-2} (1018 F g^{-1}) at a current density of 1 mA cm^{-2} and volumetric capacitance in terms of 29.1 F cm^{-3} were also calculated to provide further information. Furthermore, about 57.14% of capacitance of the nickel foam wt4 is retained when the current density is increased from 1 to 20 mA cm^{-2}. The obtained capacitive performance is significantly higher than that of $Ni(OH)_2$ nanosheets using $Fe(NO_3)_3$ as the oxidant and Ni foam as nickel source in Hydrothermal process [3, 28].

Electrochemical stability of the $Ni(OH)_2$ microrods was further investigated by means of GCD process. It can be seen in Fig. 6a that the capacitance increases slightly at 100 cycles due to the gradual activation behaviour of the active material [28, 29]. The electrode material fully activates itself through ion insertion and de-intercalation. The capacitance is stabilized in the last 100 cycles and the overall capacitance loss of the nickel foam wt4 is about 27.1% after 3000 cycles at a current density of 10 mA cm^{-2}. The symmetric GCD curves (the inset in Fig. 6a) of the initial and last three cycles can further prove the excellent charge-discharge stability. The Nyquist plots are presented in Fig. 6b to assess the electrochemical behavior of the processed nickel foams. The EIS data was fitted by an equivalent circuit consisting of the equivalent series resistance (*Rs*), the charge transfer resistance at electrode−electrolyte interface during electrochemical redox reaction (*Rct*), the element of double-layer capacitance (C_{dl}), the element of

pseudocapacitance (C_L) from redox process of the electrode, the Warburg diffusion impedance within the electrode (Z_w), as shown in the upper inset in Fig. 6b [30, 31]. The equivalent series resistance, a combination result of electrolyte resistance, intrinsic resistance of electrode and contact resistance between electrode and Ni foam, is determined by the point of intersection with the x-axis. Clearly, all samples present an extremely low equivalent series resistance while the smallest ESR of 0.5 Ω was observed in nickel foam wt4 (the inset in Fig. 6b), indicating the compact contact and optimized density of the $Ni(OH)_2$ microrods on Ni foam. It is well known that the diameter of semi-circles and straight line correspond to the charge transfer resistance and diffusion resistance. Obviously, all samples exhibit a rapid charge transfer process because no prominent semi-circular arc was observed in the high-frequency region. In the low frequency range, the largest slope of straight line corresponds to the lowest diffusive resistance of nickel foam wt4 as well.

4. Conclusions

In summary, one-step hydrothermal approach has been developed to synthesize hexagonal prism-like $Ni(OH)_2$ microrods on nickel foam, which directly serves as nickel source and 3D scaffold for $Ni(OH)_2$ growth to from a binder-free electrode. The surface morphology of processed nickel foam is strongly dependent on the hydrogen peroxide concentration. Benefiting from the direct contact with the substrate, the optimized $Ni(OH)_2$-coated nickel foam delivers an extremely low series resistance of 0.5 Ω, remarkable areal capacitance of 1.598 C cm^{-2} at 1 mA cm^{-2} with excellent cycling stability of 72.9% after 3000 GCD cycles. This report demonstrates an effective route to fabricate hexagonal prism-like $Ni(OH)_2$ microrods grown on nickel foam, which show great potential as a pseudocapacitor electrode.

Acknowledgments

This research was supported by the National Natural Science Foundation of China (61674113, 51622507, and 61471255), and Scientific and Technological Innovation Programs of Higher Education Institutions in Shanxi Province, China (2016138). The author KW acknowledged financial supporting from Norwegian Research Council-FRINATEK programme (231416/F20). We also thank Prof. Richard WilliamNelson's kindness forproof-reading.

References

[1]. J. Xu, Y. Sun, M. Lu, L. Wang, J. Zhang, J. Qian, X. Liu, Fabrication of hierarchical $MnMoO_4 \cdot H_2O@MnO_2$ core-shell nanosheet arrays on nickel foam as an advanced electrode for asymmetric supercapacitors, Chemical Engineering Journal 334 (2018) 1466-1476.

[2]. L. Lv, K. Xu, C. Wang, H. Wan, Y. Ruan, J. Liu, R. Zou, L. Miao, K. Ostrikov, Y. Lan, J. Jiang, Intercalation of Glucose in NiMn-Layered Double Hydroxide Nanosheets: an Effective Path Way towards Battery-type Electrodes with Enhanced Performance, Electrochimica Acta 216 (2016) 35-43.

[3]. Z. Chang, T. Li, G. Li, K. Wang, One-pot in-situ synthesis of $Ni(OH)_2$–$NiFe_2O_4$ nanosheet arrays on nickel foam as binder-free electrodes for supercapacitors, Journal of Materials Science: Materials in Electronics 30 (2018) 600-608.

[4]. Y. Ruan, L. Lv, Z. Li, C. Wang, J. Jiang, Ni nanoparticles@Ni-Mo nitride nanorod arrays: a novel 3D-network hierarchical structure for high areal capacitance hybrid supercapacitors, Nanoscale 9 (2017) 18032-18041.

[5]. J. Zhao, Y. Li, G. Wang, T. Wei, Z. Liu, K. Cheng, K. Ye, K. Zhu, D. Cao, Z. Fan, Enabling high-volumetric-energy-density supercapacitors: designing open, low-tortuosity heteroatom-doped porous carbon-tube bundle electrodes, Journal of Materials Chemistry A 5 (2017) 23085-23093.

[6]. Y. Wang, Z. Yin, Z. Wang, X. Li, H. Guo, J. Wang, D. Zhang, Facile construction of $Co(OH)_2@Ni(OH)_2$ core-shell nanosheets on nickel foam as three dimensional free-standing electrode for supercapacitors, Electrochimica Acta 293 (2019) 40-46.

[7]. M. Yan, Y. Yao, J. Wen, L. Long, M. Kong, G. Zhang, X. Liao, G. Yin, Z. Huang, Construction of a Hierarchical $NiCo_2S_4$@PPy Core-Shell Heterostructure Nanotube Array on Ni Foam for a High-Performance Asymmetric Supercapacitor, ACS Appl Mater Interfaces 8 (2016) 24525-24535.

[8]. H. Li, X. Li, J. Liang, Y. Chen, Hydrous RuO_2- Decorated MXene Coordinating with Silver Nanowire Inks Enabling Fully Printed Micro- Supercapacitors with Extraordinary Volumetric Performance, Advanced Energy Materials (2019) 1803987.

[9]. Y. Xie, C. Yang, P. Chen, D. Yuan, K. Guo, MnO_2-decorated hierarchical porous carbon composites for high-performance asymmetric supercapacitors, Journal of Power Sources 425 (2019) 1-9.

[10]. Y. Ouyang, R. Huang, X. Xia, H. Ye, X. Jiao, L. Wang, W. Lei, Q. Hao, Hierarchical structure electrodes of NiO ultrathin nanosheets anchored to $NiCo_2O_4$ on carbon cloth with excellent cycle stability for asymmetric supercapacitors, Chemical Engineering Journal 355 (2019) 416-427.

[11]. L. Li, J. Xu, J. Lei, J. Zhang, F. McLarnon, Z. Wei, N. Li, F. Pan, A one-step, cost-effective green method to in situ fabricate $Ni(OH)_2$ hexagonal platelets on Ni foam as binder-free supercapacitor electrode materials, Journal of Materials Chemistry A 3 (2015) 1953-1960.

[12]. B. Kirubasankar, P. Palanisamy, S. Arunachalam, V. Murugadoss, S. Angaiah, 2D $MoSe_2$-$Ni(OH)_2$ nanohybrid as an efficient electrode material with high rate capability for asymmetric supercapacitor applications, Chemical Engineering Journal 355 (2019) 881-890.

[13]. X. Xiong, D. Ding, D. Chen, G. Waller, Y. Bu, Z. Wang, M. Liu, Three-dimensional ultrathin $Ni(OH)_2$ nanosheets grown on nickel foam for high-performance supercapacitors, Nano Energy 11 (2015) 154-161.

[14]. H. Sun, S. Liu, Q. Lu, H. Zhong, Template-synthesis of hierarchical $Ni(OH)_2$ hollow spheres with excellent performance as supercapacitor, Materials Letters 128 (2014) 136-139.

[15]. J. Liang, B. Dong, S. Ding, C. Li, B.Q. Li, J. Li, G. Yang, Facile construction of ultrathin standing α-$Ni(OH)_2$ nanosheets on halloysite nanotubes and their enhanced electrochemical capacitance, Journal of Materials Chemistry A 2 (2014) 11299-11304.

[16]. H. Zhang, X. Zhang, D. Zhang, X. Sun, H. Lin, C. Wang, Y. Ma, One-step electrophoretic deposition of reduced graphene oxide and $Ni(OH)_2$ composite films for controlled syntheses supercapacitor electrodes, The Journal of Physical Chemistry B 117 (2012) 1616-1627.

[17]. D.S. Hall, D.J. Lockwood, C. Bock, B.R. MacDougall, Nickel hydroxides and related materials: a review of their structures, synthesis and properties, Proceedings of the Royal Society A: Mathematical, Physical and Engineering Sciences 471 (2015) 20140792.

[18]. P. Lu, F. Liu, D. Xue, H. Yang, Y. Liu, Phase selective route to $Ni(OH)_2$ with enhanced supercapacitance: performance dependent hydrolysis of $Ni(Ac)_2$ at hydrothermal conditions, Electrochimica Acta 78 (2012) 1-10.

[19]. J. Yan, W. Sun, T. Wei, Q. Zhang, Z. Fan, F. Wei, Fabrication and electrochemical performances of hierarchical porous $Ni(OH)_2$ nanoflakes anchored on graphene sheets, Journal of Materials Chemistry 22 (2012) 11494-11502.

[20]. R. Vasireddi, B. Javvaji, H. Vardhan, D. Mahapatra, G. Hegde, Growth of zinc oxide nanorod structures: pressure controlled hydrothermal process and growth mechanism, Journal of materials science 52 (2017) 2007-2020.

[21]. Y. Khan, S. Hussain, F. Söderlind, P.-O. Käll, M.A. Abbasi, S.K. Durrani, Honeycomb β-$Ni(OH)_2$ films grown on 3D nickel foam substrates at low temperature, Materials Letters 69 (2012) 37-40.

[22]. K. Li, J. Ma, X. Guan, H. He, M. Wang, G. Zhang, F. Zhang, X. Fan, W. Peng, Y. Li, 3D self-supported $Ni(PO_3)_2$-MoO_3 nanorods anchored on nickel foam for highly efficient overall water splitting, Nanoscale 10 (2018) 22173-22179.

[23]. J.M. Campos- Martin, G. Blanco- Brieva, J.L. Fierro, Hydrogen peroxide synthesis: an outlook beyond the anthraquinone process, Angewandte Chemie International Edition 45 (2006) 6962-6984.

[24]. D.-C. Liu, L.-M. Cao, Z.-M. Luo, D.-C. Zhong, J.-B. Tan, T.-B. Lu, An in situ generated amorphous CoFePi and crystalline $Ni(PO_3)_2$ heterojunction as an efficient electrocatalyst for oxygen evolution, Journal of Materials Chemistry A 6 (2018) 24920-24927.

[25]. X. Cheng, Z. Pan, C. Lei, Y. Jin, B. Yang, Z. Li, X. Zhang, L. Lei, C. Yuan, Y. Hou, A strongly coupled 3D ternary Fe_2O_3@Ni_2P/$Ni(PO_3)_2$ hybrid for enhanced electrocatalytic oxygen evolution at ultra-high current densities, Journal of Materials Chemistry A 7 (2019) 965-971.

[26]. Y. Gogotsi, R.M. Penner, Energy Storage in Nanomaterials - Capacitive, Pseudocapacitive, or Battery-like?, ACS Nano 12 (2018) 2081-2083.

[27]. J. Li, Z. Liu, Q. Zhang, Y. Cheng, B. Zhao, S. Dai, H.-H. Wu, K. Zhang, D. Ding, Y. Wu, M. Liu, M.-S. Wang, Anion and cation substitution in transition-metal oxides nanosheets for high-performance hybrid supercapacitors, Nano Energy 57 (2019) 22-33.

[28]. L. Peng, L. Lv, H. Wan, Y. Ruan, X. Ji, J. Liu, L. Miao, C. Wang, J. Jiang, Understanding the electrochemical activation behavior of $Co(OH)_2$ nanotubes during the ion-exchange process, Materials Today Energy 4 (2017) 122-131.

[29]. H. Chen, J. Jiang, L. Zhang, T. Qi, D. Xia, H. Wan, Facilely synthesized porous $NiCo_2O_4$ flowerlike nanostructure for high-rate supercapacitors, Journal of Power Sources 248 (2014) 28-36.

[30]. J. Xu, Y. Sun, M. Lu, L. Wang, J. Zhang, E. Tao, J. Qian, X. Liu, Fabrication of the porous $MnCo_2O_4$ nanorod arrays on Ni foam as an advanced electrode for asymmetric supercapacitors, Acta Materialia 152 (2018) 162-174.

[31]. J. Xu, Y. Sun, M. Lu, L. Wang, J. Zhang, X. Liu, One-step electrodeposition fabrication of Ni_3S_2 nanosheet arrays on Ni foam as an advanced electrode for asymmetric supercapacitors, Science China Materials 62 (2018) 699-710.

[32]. X. Xiong, Z. Wang, H. Guo, X. Li, Facile synthesis of ultrathin nickel hydroxides nanoflakes on nickel foam for high-performance supercapacitors, Materials Letters 138 (2015) 5-8.

[33]. Q. Zhou, M. Cui, K. Tao, Y. Yang, X. Liu, L. Kang, High areal capacitance three-dimensional Ni@$Ni(OH)_2$ foams via in situ oxidizing Ni foams in mild aqueous solution, Applied Surface Science 365 (2016) 125-130.

[34]. J.M. Xu, K.Y. Ma, J.P. Cheng, Controllable in situ synthesis of $Ni(OH)_2$ and NiO films on nickel foam as additive-free electrodes for electrochemical capacitors, Journal of Alloys and Compounds 653 (2015)

88-94.

[35]. S.R. Ede, S. Anantharaj, K.T. Kumaran, S. Mishra, S. Kundu, One step synthesis of Ni/$Ni(OH)_2$ nano sheets (NSs) and their application in asymmetric supercapacitors, RSC Advances 7 (2017) 5898-5911.

Fig. 1 Fabrication procedureand schematic illustration for the hexagonal prism−like $Ni(OH)_2$ microrods by hydrothermal process.

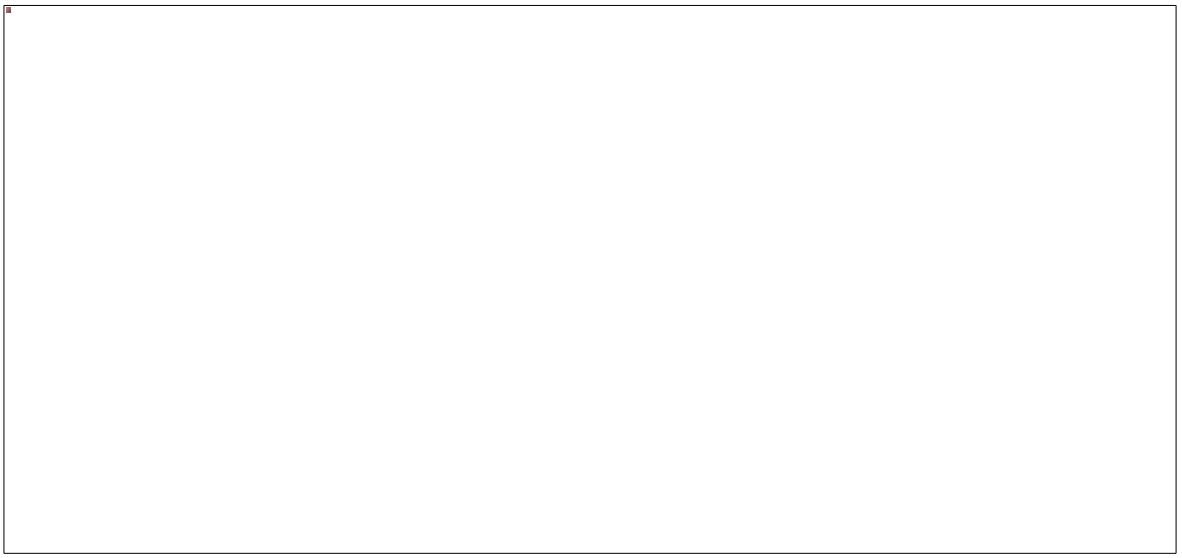

Fig. 2 SEM images of $Ni(OH)_2$ samples (a–f). (e) The figure is a closer examination of morphology of the $Ni(OH)_2$ microrods (sample wt4).

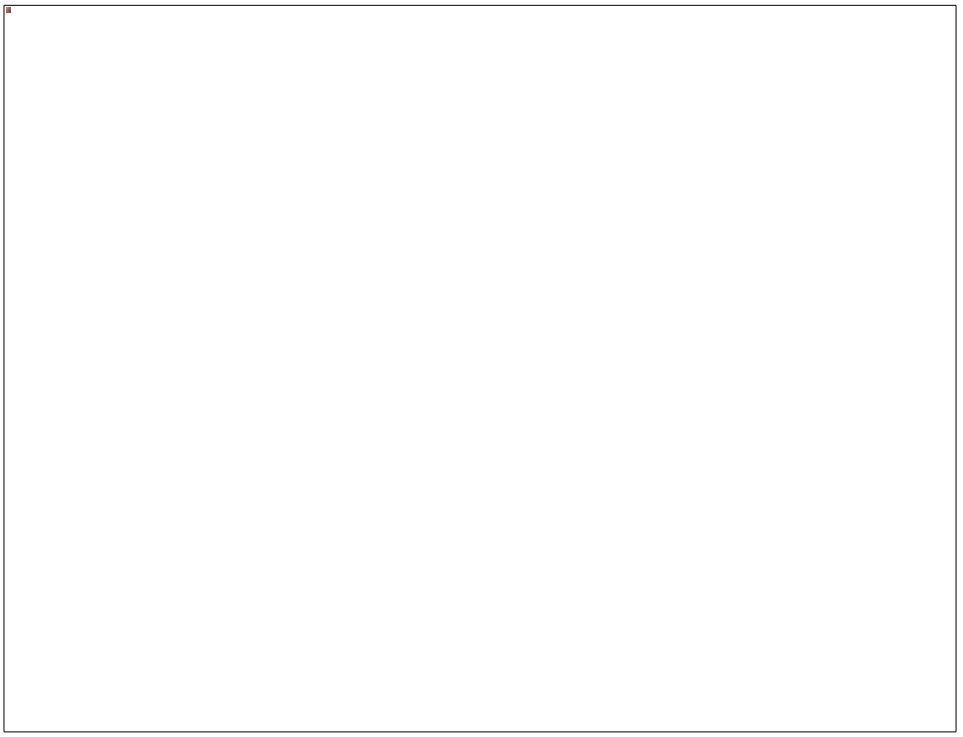

Fig. 3 XRD pattern of the nickel foam oxidized by hydrogen peroxide solution at a concentration of 20%.

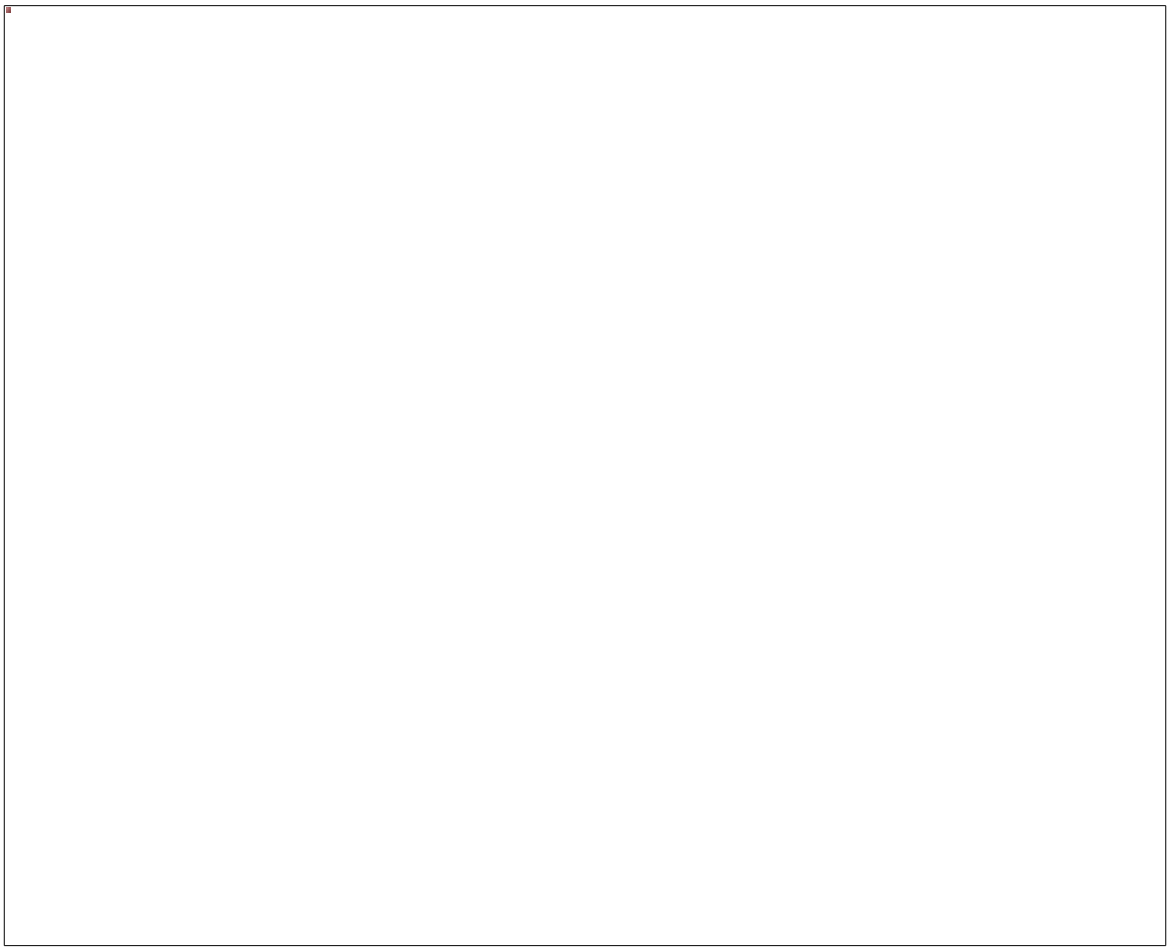

Fig. 4 XPS results of the pure nickel foam oxidized by hydrogen peroxide solution at a concentration of 20%: (a) survey scan, (b) Ni *2p*, (c) O *1s*, (d) P *2p*.

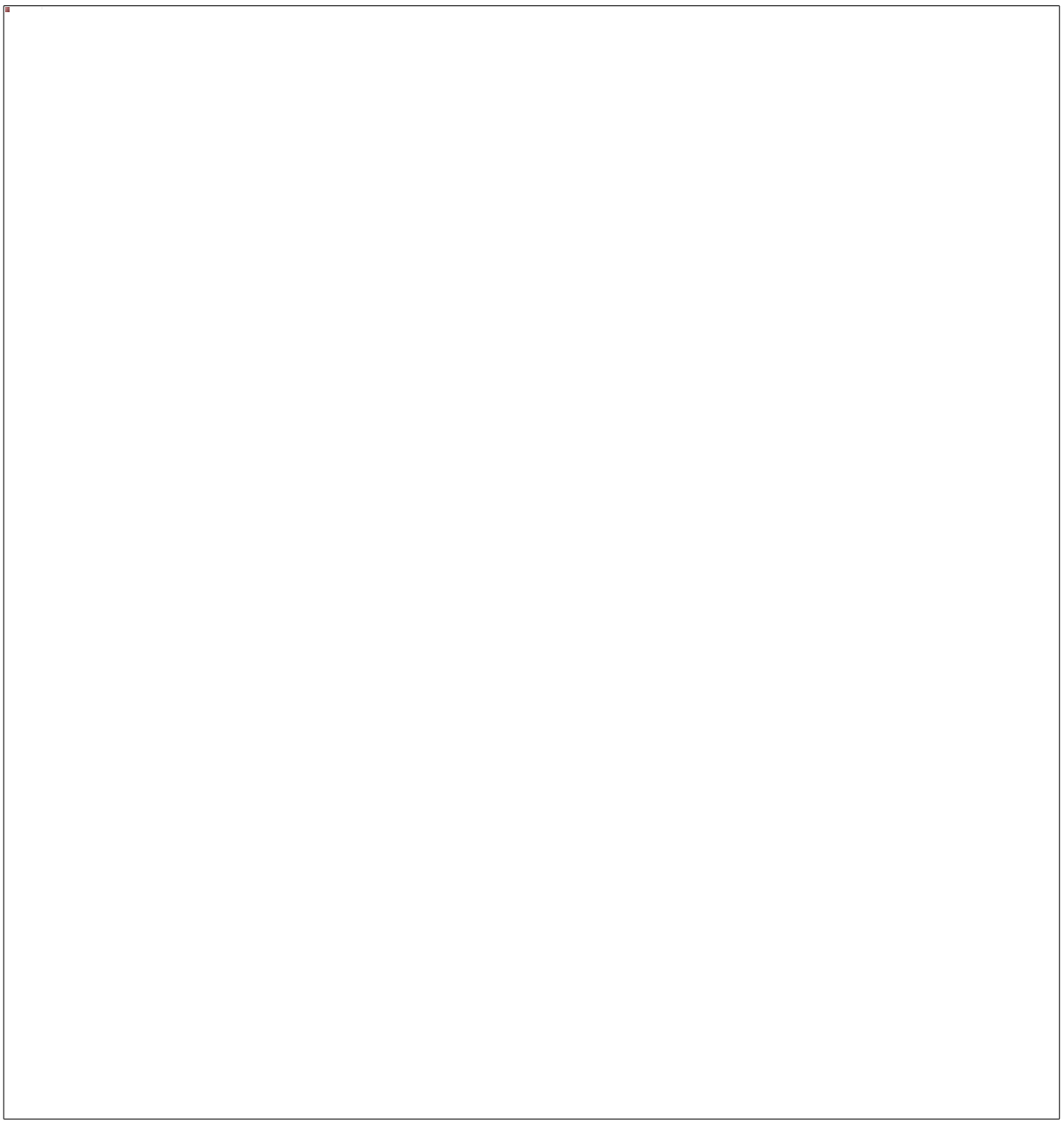

Fig. 5 (a) CV curves of the example wt1, wt2, wt3, wt4 and wt5 electrodes obtained at a scan rate of 20 mV s^{-1}. (b) CV curves of the sample wt4 electrode at different scan rates. (c) log (peak current, *i*) versus log (scan rate, *v*). (d) GCD curves of the example wt1, wt2, wt3, wt4 and wt5 electrodes obtained at current density of 5 mA cm^{-2}. (e) GCD curves of the example wt4 electrode at different current densities. (f) Areal capacitance of the electrodes as a function of the current density.

Fig. 6 (a) Cycling performance of the example wt4 at a current density of 10 mA cm^{-2} (the inset pictures are the galvanostatic charge−discharge curves of first and last three cycles, respectively). (b) Nyquist impedance plots of the five electrodes (the upper inset is the proposed equivalent circuit and the lower inset is the enlarged Nyquist plots in high frequency region).